In situ investigation of rapid subsurface flow: Identification of relevant spatial structures beyond heterogeneity

Conrad Jackisch[1], Lisa Angermann[2], Niklas Allroggen[3], Matthias Sprenger[4,5], Theresa Blume[2], Markus Weiler[4], Jens Tronicke[3], and Erwin Zehe[1]

[1]Karlsruhe Institute of Technology (KIT), Institute for Water and River Basin Management, Chair of Hydrology, Karlsruhe, Germany
[2]Helmholtz Centre Potsdam, GFZ German Research Centre for Geosciences, Section Hydrology, Potsdam, Germany
[3]University of Potsdam, Institute of Earth and Environmental Science, Potsdam, Germany
[4]University of Freiburg, Institute of Geo- and Environmental Natural Sciences, Chair of Hydrology, Freiburg, Germany
[5]University of Aberdeen, School of Geosciences, Geography & Environment, Aberdeen, Scotland, UK

Correspondence to: Conrad Jackisch (jackisch@kit.edu)

Abstract. Rapid subsurface flow in structured soils facilitates fast vertical and lateral redistribution of event water. Despite their significance and omnipresence the related processes are challenging hydrological exploration, monitoring, modeling and theory. One reason for this is that flow processes at high velocities are difficult to observe in the subsurface. Another reason is that advective flow is channeled in distinct connected structures several orders of magnitude smaller than commonly re-
5 solved observation volumes. This is the second part of a companion paper with a focus on *in situ* experimental exploration of rapid subsurface flow. Complementary to the temporal dynamics, this study looks into the identification of spatially organized structures. We present a bottom-up approach with point-scale measurements, plot-scale multi-tracer experiments and a hillslope-scale irrigation experiment. Special emphasis is given to the employed 2D and 3D time-lapse ground penetrating radar monitoring under field conditions on forested, young soils on periglacial slope deposits. The study highlights the difficulty to
10 draw conclusions beyond overall heterogeneity from point observations in a basically unknown and structured domain. We also spotlight the challenge to identify relevant structures based on a single quasi-static exploration. A coherent combination of different hydrological and geophysical methods to monitor the system under driven conditions was key to reduce ambiguity in the identification of hydrologically relevant structures and the overall process understanding.

1 Introduction

1.1 Rapid subsurface flow structure identification

Preferential or rapid subsurface flow dominates the redistribution of event water and characterizes most catchments (Flury et al., 1994; Uhlenbrook, 2006). Channelled through biogene structures, such as earthworm burrows (Blouin et al., 2013; Palm et al., 2012; van Schaik et al., 2014) and plant roots (Nadezhdina et al., 2010), and geogene structures like voids in periglacial cover beds (Heller, 2012), it is partially bypassing large sections of the soil which is a long-standing issue in hydrology. Beven and Germann (1982, 2013) recently framed the discussion by resuming that macropores and preferential flow are still not given the attention appropriate to their significance in all areas of soil and catchment hydrology.

With regard to identification and characterization of specific flow paths, a large spectrum of methods is applied to investigate subsurface connectivity (Blume and van Meerveld, 2015). Dye staining has evolved as common practise since its first applications (Flury et al., 1994) for a retrospective imaging of preferential flow paths. This provides valuable information but requires strong assumptions about macropore-matrix interaction, time of fixation and recoverability. Furthermore, salt tracer breakthrough curves are commonly used (e.g. Wienhöfer and Zehe, 2014) and provide quantitative information over the course of rapid flow events. However, such measurements can only capture signals in an integral form. Very few studies actually examine rapid subsurface flow from the plot to the hillslope and resolve the respective flow paths (e.g. Anderson et al., 2009; McDonnell et al., 2011; Guo et al., 2014).

Besides the general acknowledgement of preferential flow as omni-present under non-equilibrium conditions (Uhlenbrook, 2006; Jarvis, 2007; Zehe et al., 2013; Germann, 2014) and considerable efforts to quantify it (Allaire et al., 2009), our current theories are mainly shaped by rather few experiments in experimental basins: Russell Creek, British Columbia, Canada (Anderson et al., 2009), Maimai Experimental Watershed, New Zealand (Graham et al., 2010), Panola Mountain Research Watershed, Georgia, USA (van Meerveld et al., 2015), H. J. Andrews Experimental Forest, Oregon, USA (McGuire and McDonnell, 2010). In far more studies models are used to examine the characteristics of an additional fast flow domain which is often observed as double peaks in discharge and tracer breakthrough (e.g. Schotanus et al., 2012; Klaus et al., 2013). Although these model studies have been very successful (Superflex in the same basin as this study (Fenicia et al., 2014), Catflow to reproduce an irrigation experiment at the hillslope-scale (Klaus and Zehe, 2010), explicit 3D structure representation (Vogel et al., 2006) and many more) they require strong assumptions about the development of connectivity and the interaction between matrix and structures (Gerke, 2006).

At smaller scales the issue is quite similar: Rather few experiments are reported that investigate preferential flow in structures and exchange with the matrix (Jarvis, 2007). At the same time a considerable body of models and theoretical concepts has evolved: Stochastic stream tubes (Jury and Roth, 1990), the scale way idea (Vogel and Roth, 2003), dual porosity and permeability approaches (Gerke, 2006), and spatially explicit representation of macropores as vertically and laterally connected flow paths (Vogel et al., 2006; Sander and Gerke, 2009; Klaus and Zehe, 2011).

While the models require specific parameters about the site under study which are coherent with their conceptual assumptions or modeller's perception (Holländer et al., 2014), also the experiments are strongly shaped by our perceptual model about the processes. With this, the matter of model adequacy is not restricted to numerical aspects alone (Gupta et al., 2012). Methodologically, we lack approaches that provide *in situ* imaging of subsurface flow processes as basis to reduce ambiguity

5 of measurements and to constrain the process conceptualization in heterogeneous and structured soils.

1.2 Objectives, hypotheses and approach

Complementary to the temporal perspective on preferential flow path detection and characterization by Angermann et al. (2016, this issue), this study looks at the spatial aspects of preferential flow in the young and highly structured periglacial soils of the Colpach basin in western Luxembourg. In the past decade a number of studies were conducted in this catchment, focussing

10 on the general runoff generation characteristics and process conceptualization (van den Bos et al., 2006; Juilleret et al., 2011; Wrede et al., 2015). We seek to answer the following questions: Which structures become relevant for the observed rapid subsurface flow reaction? By which means can the structures be identified? Where and how establish connected flow fields? What are the characteristics of the hydrologically active structures?

The temporal aspect to this study (Angermann et al., 2016, this issue) has pinpointed that although operating at highest

15 achievable resolutions in time and space the picture of the subsurface flow structures remains rather blurred. This second part will highlight the spatial domain of the study and link exploration methods from static singular point measurements to characterization of 3D flow fields.

We start with a large number of hydrological field and laboratory measurements which eventually can only frame local heterogeneity. The structures remained rather unknown and hardly identifiable even by precise and distributed but static meth-

20 ods like 3D GPR surveying. Irrigation experiments as analyses under driven conditions generate much closer insight into the processes and their temporal development. At the plot scale we identify how local structures are activated for fast vertical and lateral redistribution. A large irrigation experiment at the hillslope scale extends and complements the previous findings.

By coherently combining multiple methods in the experiments we establish a unique basis to combine findings from local, plot and hillslope scale.

2 Methods

In order to investigate the role and characteristics of preferential flow, multiple exploratory and experimental approaches have been chosen:

1 Exploration was based on a number of *in situ* measurements of infiltration capacity, and saturated hydraulic conductivity in
5   different depth levels. Undisturbed soil samples were analysed for soil water retention, bulk density and texture in the laboratory. In addition 3D GPR surveys at the plot and hillslope scale were conducted.

2 Plot-scale processes were observed with multi-tracer irrigation experiments exhibiting the preferential flow patterns by Brilliant Blue dye stains. The flow field was further quantified with Bromide salt tracer and stable isotopes in the soil water. Continuous TDR soil moisture monitoring and time-lapse 3D GPR were used to extend and refine the observations
10   in time and space.

3 The local findings were extended to the hillslope-scale by an irrigation experiment with dense TDR monitoring and multiple 2D time-lapse GPR transects as presented by Angermann et al. (2016, this issue). In the study at hand, additional aspects on spatial structures are emphasized.

2.1 Local exploration

15 Infiltration capacity was measured at 40 sites along 2 catenas in the upper Colpach River basin with a Hood Tension-Infiltrometer IL-2700 (UGT GmbH). The nested sampling design was alined to the monitoring network of the CAOS project observatory (Zehe et al., 2014) with 3-8 samples in a radius of 20 m around the monitoring sensor clusters (D, E, G, H, I) and a distance of some 80 m to 200 m between the latter.

    The infiltrometer employs a tension chamber (12.4 cm radius) as infiltration water supply. Inside the chamber, a defined low
20 negative pressure head can be established, which allows a precise measurement of infiltration capacity at different tensions. 3 to 5 tension levels between 0 and 5.5 cm water column were applied at each spot.

    In addition to infiltration capacity at the surface we used a Compact Constant Head Permeameter (CCHP, Ksat Inc.) for determination of saturated hydraulic conductivity in 32 borehole profiles with 3 to 7 depth levels of about 20 cm increments with the lowest level at a depth where further hand-drilling was inhibited by stones. The sampling layout followed a similar
25 pattern as for the infiltration measurements but with small-scale pairs of two profiles (1 m apart).

    The permeameter establishes a constant water level (10.5 cm in our cases) above the bottom of a borehole (r=2.5 cm). The outflow is used in the Glover solution to calculate saturated hydraulic conductivity (k_{sat}) (Amoozegar, 1989). The Glover solution requires isotropic conditions which are by no means given at the study site. Thus, the resulting values have to be taken with some precaution if one seeks to derive proper estimates for k_{sat}. In this study, they are used for relative inter-comparison
30 to detect characteristic profiles and conductive layers.

    The *in-situ* measurements were accompanied by a series of percussion drilled soil cores (drill head diameter of 40 mm) to reference possible soil layers to findings from the quantitative exploration. Moreover, 51 undisturbed soil ring samples (250 mL,

within the top $0.7\,\mathrm{m}$) were taken and analyzed for saturated hydraulic conductivity (Ksat, UMS GmbH), soil water retention properties (Hyprop, UMS GmbH and WP4C Decagon Devices Inc.), bulk density, pH and texture (ISO 11277, wet sieving and sedimentation).

2.2 Plot-scale tracer experiments

5   In order to explore the effect and characteristics of rapid subsurface flow and the macropore network we conducted three plot-scale irrigation experiments. The general setup is very similar to the setup described by Allroggen et al. (2015b), van Schaik (2009) and Kasteel et al. (2002): Three plots of $1\,\mathrm{m}^2$ size were irrigated for $1\,\mathrm{h}$ with an intensity of $50\,\mathrm{mm\,h}^{-1}$, $30\,\mathrm{mm\,h}^{-1}$ and $50\,\mathrm{mm\,h}^{-1}$. The relatively high rates were chosen to activate all potential flow paths and thereby establishing connectivity. The irrigation was accomplished by spray irrigation (full-cone nozzle Spraying Systems Co.) using a wind-protection tent. Brilliant

10   Blue dye tracer ($4\,\mathrm{g\,L}^{-1}$) and Bromide salt ($5\,\mathrm{g\,L}^{-1}$ Potassium bromide) were used for qualitative and quantitative reference, respectively.

   In addition, soil moisture was monitored throughout the experiments through continuous TDR measurements in an access tube (Pico IPH, IMKO GmbH) with $4.2\,\mathrm{cm}$ diameter. The sensor was lowered to the respective depth and measured an integral of about $1.05\,\mathrm{L}$ (depth increment of $18\,\mathrm{cm}$, mean signal penetration of $5.5\,\mathrm{cm}$). The resulting measurement interval for each

15   depth level was $5\,\mathrm{min}$ to $10\,\mathrm{min}$.

   $2\,\mathrm{h}$ after the end of each irrigation, a percussion drilled soil core was taken (drill head diameter of $8\,\mathrm{cm}$) and sampled in $5\,\mathrm{cm}$ depth increments down to $1\,\mathrm{m}$. The plot was excavated $24\,\mathrm{h}$ after irrigation for vertical and horizontal recovery of Brilliant Blue stains. At the vertical excavation face in the center of the irrigation plot, samples of $66\,\mathrm{mL}$ soil were taken in a $5\,\mathrm{cm}$ grid with 5 columns and 14 to 21 rows. All samples were analyzed for Bromide (Br^-). This was done by suspending the oven dried

20   samples in $150\,\mathrm{mL}$ de-ionised water ($72\,\mathrm{h}$ in overhead shaker at 9 rotations per minute). The samples were then left 4 days for sedimentation to exfiltrate the excess through a) filtration paper ($5\,\mathrm{\mu m}$ to $13\,\mathrm{\mu m}$) and b) $0.45\,\mathrm{\mu m}$ PP micro-filter. The extracts were analyzed in an Ion Chromatograph (Metrohm 790 Personal IC) with an anion separation column (Metrosep A Supp 4 - 250/4.0) for Br^- concentration.

   A recovery coefficient is calculated as proportion of recovered mass of Br^- in the soil samples scaled to the total irrigated

25   area times the depth of the lowest sample. Through this we neglect lateral flow from the irrigation spot and further percolation in the calculation. We also assume the samples to be representative for the whole affected soil volume.

   Prior to the Bromide analysis, the percussion drilled soil core samples were also analyzed for their stable isotopic composition ($\delta^{18}O$ and $\delta^2 H$) of the pore water. The pore water isotope analysis was done with the direct equilibration method as proposed by Wassenaar et al. (2008) and described in detail by Sprenger et al. (2015b) using a wavelength-scanned cavity ring-

30   down spectrometer (Picarro Inc.). The precision for the method is reported to be $0.31\,‰$ for $\delta^{18}O$ and $1.16\,‰$ for $\delta^2 H$ (Sprenger et al., 2015a). The measured isotopic signal is given relative to the Vienna Standard Mean Ocean Water. As pre-experiment reference, a fourth core has been sampled prior to the experiments about $3\,\mathrm{m}$ upslope.

Hydrology and
Earth System
Sciences

Open Access

Discussions

EGU

We calculate the volumetric event water portion [-] in the soil water as:

$$\frac{\Theta_{event}}{\Theta_{2h}} = \frac{\Theta_{2h} \cdot \delta^2 H_{2h} - \Theta_{pre} \cdot \delta^2 H_{pre}}{\Theta_{2h} \cdot \delta^2 H_{event}} \tag{1}$$

with $\delta^2 H$ as Deuterium composition [‰] in the pre-event reference sample (pre), in the core sample 2 h after irrigation start ($2h$), and in the irrigation water ($event$). The amount of soil water is given as Θ [mm].

5   The experiments are also monitored by 3D time-lapse GPR (Ground Penetrating Radar) measurements as described by Allroggen et al. (2015b). We employed a PulseEKKO Pro GPR system (Sensors and Software Inc.) equipped with 500 MHz shielded antennas with constant offset of 0.18 m. Sampling interval was set to 0.1 ns, recording a total trace length of 100 ns at an internal stacking rate of 8. Since precise positioning and accurate repeatability are key requirements, we used a kinematic survey approach relying on an automatic-tracking total station (Leica Geosystems AG), providing sub-centimeter coordinates,

10 in combination with a portable measuring platform as presented by Allroggen et al. (2015b).

Using this setup, we acquired one 3D GPR cube before irrigation, one directly after the end of irrigation, and a last one 20 h after irrigation for each irrigation plot. One survey took about 45 min. As presented by Allroggen and Tronicke (2016), we calculate the structural similarity attribute to identify differences between the individual data cubes after a processing which includes bandpass filtering, exponential scaling, gridding to a regular 2 cm grid and a topographic migration approach. This

15 technique is further explained in section 2.3.4.

2.3   Hillslope-scale irrigation experiment

The general setup of the irrigation experiment at a hillslope in the Holtz sub-basin is described in detail by Angermann et al. (2016, this issue). This experiment targeted the *in situ* observation and imaging of subsurface flow processes and identification of structures at a larger scale. Therefore we rearranged elements and methods from the plot-scale experiments to three diverting

20 transects to monitor soil moisture profiles with TDR along the catena, and four perpendicular transects with 2D time-lapse GPR measurements.

2.3.1   Preparatory 3D GPR Survey

As a reference for further interpretation of the experimental findings a 3D GPR survey of the hillslope was conducted prior to the irrigation experiment. The GPR data processing relies on a standard processing scheme including bandpass filtering,

25 zero time correction, envelope based automatic scaling, gridding to a regular 0.03 m by 0.1 m grid, inline fk-filtering and a 3D topographic migration approach as presented by Allroggen et al. (2015a), using an appropriate constant velocity of 0.07 m ns^{-1}.

For structural analysis, the processed data are imported into the OpenDtect software (dGB Earth Sciences). A classical structural analysis based on picking continuous reflectors is limited by the lateral extend and complex reflection patterns, which dominate the data cube. Consequently, we employed an attribute supported picking approach to identify areas of high

30 reflector continuity. Potential subsurface structures are identified by visual interpretation and picking of selected reflection events. Especially a dip corrected semblance attribute provides a useful guide for identifying continuous reflection events

(Marfurt et al., 1998; Tronicke and Böniger, 2013). Low semblance indicates more complex reflection patterns caused by high internal heterogeneity, possibly influencing the subsurface flow regime.

2.3.2 Irrigation experiment and process monitoring

Based on the findings of the local exploration and plot experiments, we hypothetically setup the 2D process model CATFLOW

5 (Zehe et al., 2001) as representative hillslope for *a priori* simulation of the experiment in order to determine the required irrigation intensity, the spatial extent of the observation network, and the temporal resolution and duration of the monitoring. Using the measured topography of the experimental hillslope, mean soil water retention characteristics and different hypotheses for conductive layers the desired forcing was estimated with $30 \, \mathrm{mm \, h^{-1}}$ for about $4 \, \mathrm{h}$.

The irrigation of $141 \, \mathrm{mm}$ in $4.5 \, \mathrm{h}$ was realized by four circular irrigation sprinklers (Wobbler, Senninger Irrigation Inc.)

10 arranged to overlap at a $5 \, \mathrm{m}$ by $5 \, \mathrm{m}$ core area of relatively homogeneous intensity. While boundary effects were mitigated by an irrigated buffer zone of about $4 \, \mathrm{m}$ at the uphill and lateral borders of the core area, the downhill boundary is defined by a rain shield. This establishes a sharp transition to the non-irrigated area below. Water collected by the rain shield is routed off the experimental site. This setup is comprised with the results in Figure 7.

We continuously monitored soil moisture dynamics in a setup of 16 access tubes with 3 TDR sensors (Imko GmbH, two

15 with $12 \, \mathrm{cm}$ integration depth and one with $18 \, \mathrm{cm}$). Measurements were taken in $10 \, \mathrm{cm}$ depth increments. Five piezometers with CTD loggers (Decagon Devices Inc.) were used to measure potentially establishing shallow ephemeral groundwater. The four 2D time-lapse GPR transects were treated as *GPR-inferred trenches*. Here, the GPR acquisition unit was equipped with shielded $250 \, \mathrm{MHz}$ antennas. The data were recorded using a constant offset of $0.38 \, \mathrm{m}$, a sampling interval of $0.2 \, \mathrm{ns}$ and a time-window of $250 \, \mathrm{ns}$. Wooden guides and the automatic tracking total station guaranteed accurate and repeatable positioning with

20 sub-centimeter precision.

The stable isotope signal was measured for the natural event water, irrigation water, water from five piezometers and soil water from three successively sampled soil core profiles. The soil water isotopic composition was determined as described in section 2.2. The liquid water samples were analyzed with a vaporizer coupled to the cavity ring-down spectrometer.

2.3.3 Analysis of TDR data

25 In order to align and compare the almost 5000 individual TDR soil moisture records we resampled the data set to a regular grid in time and depth. Since the correlation length of distributed soil moisture observations is rather short and because we explicitly aim to analyze the reaction of preferential flow structures the issue of interpolation needs special attention and will be discussed in section 4.2.2.

All soil moisture measurements are converted to changes in soil moisture referenced to the state previous to irrigation onset

30 to identify activated flow paths. The individual measurements with the different probes have been resampled to a regular grid of $10 \, \mathrm{cm}$ depth and $15 \, \mathrm{min}$ time interval. With this the spatial aggregation remains below the integration length of the TDR probes. The temporal resampling and the therefore necessary linear interpolation is close to the acquisition timing of one profile (4 to

10 min each). Lateral interpolation between different TDR profiles over distances of about 1 m and above is unfeasible because a connective continuum cannot be assumed.

2.3.4 GPR transects and structural similarity attribute interpretation

The 2D time-lapse GPR data is derived from 9 repeated recordings along four vertical GPR transects. Each record is processed
5 after a standard scheme of bandpass filtering, zero time correction, exponential amplitude preserving scaling, inline fk-filtering, topographic migration with constant velocity ($0.07 \, \mathrm{m \, ns^{-1}}$), and consecutive gridding to a 2D transect with regular trace-spacing of $0.02 \, \mathrm{m}$.

Most time-lapse GPR data analyses are based on calculating trace-to-trace differences (Birken and Versteeg, 2000; Trinks et al., 2001) or picking and comparison of selected reflection events in the individual time-lapse transects (Allroggen et al.,
10 2015b; Haarder et al., 2011; Truss et al., 2007). The radargrams in the young, highly heterogeneous soils do not exhibit explicit reflectors as suitable references. In addition, the limited precision of the repeated measurements and the desired identification of lateral flow structures require an alternative approach. We use the time-lapse structural similarity attribute presented by Allroggen and Tronicke (2016).

This approach incorporates a correlation-based attribute for highlighting differences between individual GPR transects. Due
15 to the presence of remaining event water from the preceding storm event, all measurements are referenced to the last acquisition time approximately 24 h after irrigation start and about 19 h after irrigation. The resulting structural similarity attributes are used as a qualitative indicator for relative deviations from the reference state.

2.3.5 Discriminating the natural storm event and the irrigation experiment

The experiment was preceded by two strong storm events of 43 mm in total on June 20, 2013. In reference to the gauge reaction
20 the experiment was conducted shortly before the major peak of the resulting runoff reaction (Fig. 3 in Angermann et al. (2016), this issue). Accordingly, the structural similarity attributes identify responses to both drivers, the natural storm event and the irrigation experiment. To discriminate the signals we analyze the dynamics of each pixel in the GPR transects over time. The first two structural similarity attribute transects 6.5 h before and directly at irrigation start are attributed to the natural event and show an increasing similarity. Once the attribute value of a pixel decreases again (less similarity) it is attributed to the
25 irrigation. To avoid noise a threshold of 0.15 was introduced.

3 Results

3.1 Local exploration: Soil properties and subsurface structures

The results of all local measurements are compiled in Figure 1. They particularly pinpoint the heterogeneity of the soils in the studied area. Local variability is visible in the wide spread of infiltration capacity and saturated hydraulic conductivity.

5   Infiltration capacity ranges between $5 \times 10^{-5}\,\mathrm{m\,s^{-1}}$ to $5 \times 10^{-3}\,\mathrm{m\,s^{-1}}$.

Besides their spread, the values for saturated hydraulic conductivity exceed the measuring range of the constant head perme-ameter ($1 \times 10^{-8}\,\mathrm{m\,s^{-1}}$ to $1 \times 10^{-3}\,\mathrm{m\,s^{-1}}$). Figure 1B gives the mean profiles for each cluster site as large connected dots and the individual measurements as small points. While the data of the Holtz site (slope of the hillslope-scale irrigation experi-ment) suggest a conductive layer in about $0.7\,\mathrm{m}$ depth, no such general pattern is corroborated mainly due to lack of data where

10   hand-drilling was inhibited by stones.
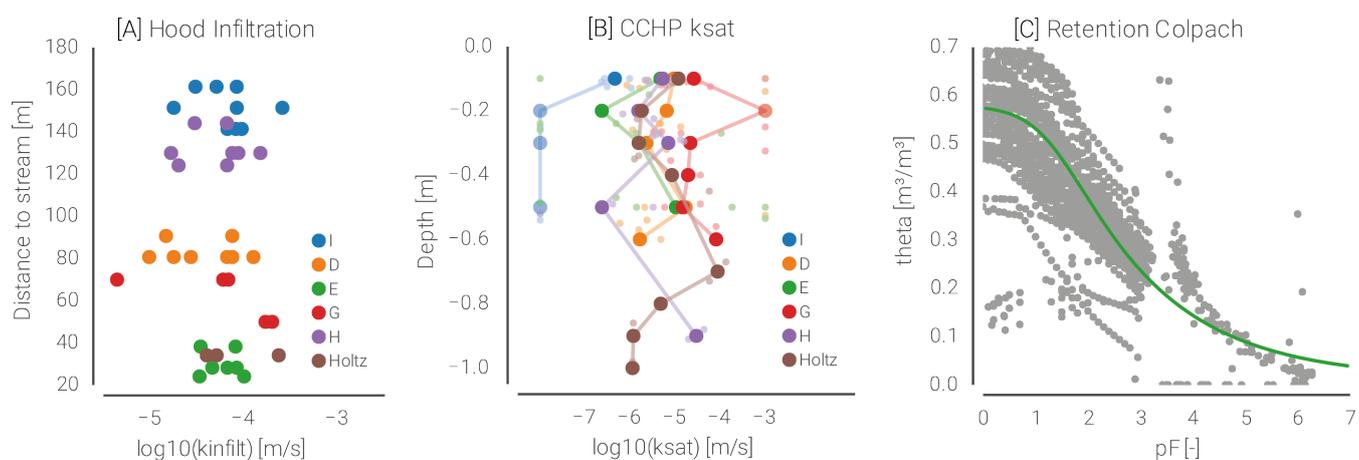
Figure 1. Local measurements of (A) infiltration capacity (Hood Infiltrometer at zero tension), (B) saturated hydraulic conductivity (Compact Constant Head Permeameter in different depth layers) local means (large connected dots) and individual measurements (small points). Transparent dots at measurement limit of device. The data are color coded according to monitoring clusters of the CAOS research group (Zehe et al., 2014). (C) Soil water retention characteristics (from $250\,\mathrm{ml}$ undisturbed soil ring samples) in the Colpach basin. Green line as maximum likelihood estimator based on all samples.

Analysis of the soil samples reveals the texture and water retention characteristics of a silty soil, which is in accordance with previous descriptions (Juilleret et al., 2011). Figure 1C presents the results from the individual sample analyses and a maximum likelihood estimator. Also here, a large spread for most of the retention spectrum is apparent which is likely attributed to the highly variable available pore space in the gravely soils. The results for infiltration capacity and hydraulic conductivity are

15   generally well above the expectations for the silty material also caused by the high porosity of the barely developed aggregated material.

The soil core samples (Figure 2) generally confirm the presence of the periglacial slope deposits by gravel bands but also show a high degree of heterogeneity. The thickness of the horizons is variable, with a humidified mineral A-horizon of up to 0.3 m. The gravel content gradually increases over depth in the Bw-horizon and further increases in the C-horizon, starting between 0.4 m and 1.1 m depth. Below the depth of 0.5 m scattered layers of weathered rock with usually horizontal orientation

5 were found in some soil cores. Percussion drilling was often inhibited at a depth between 1.5 m and 2.0 m due to even higher stone content with a more and more vertical orientation of the weathered rocks. In T7, concretions of iron and manganese oxides were found in the depth between 1.6 m and 1.9 m below ground, indicating hydromorphic conditions.
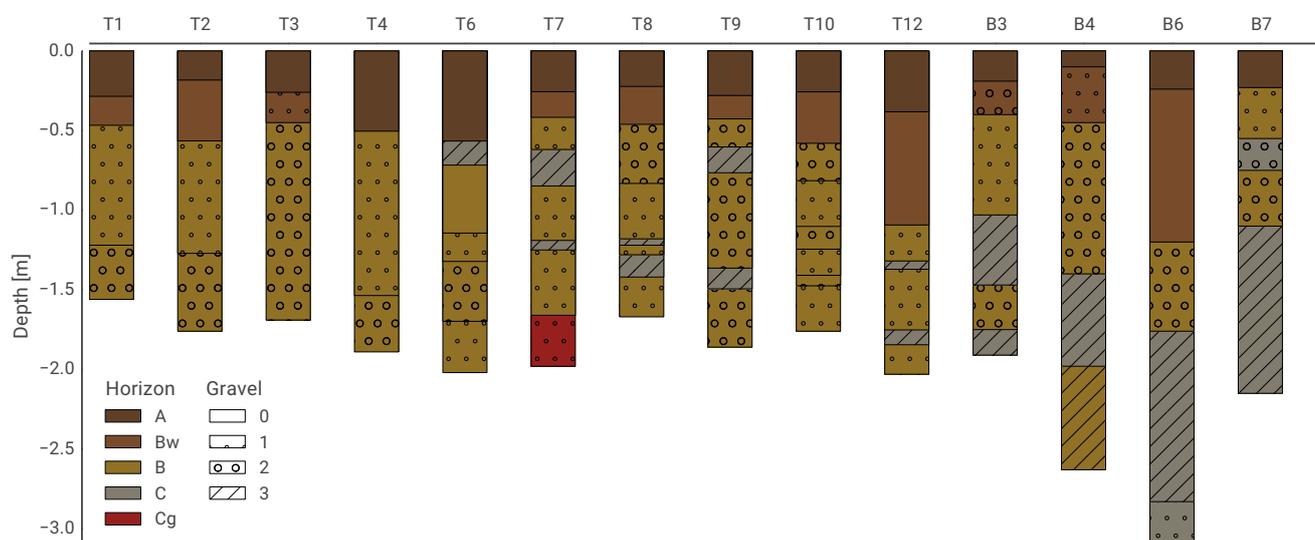
Figure 2. Soil core samples from the upper Colpach River basin. The T-nomenclature indicates cores from the installation of the TDR access tubes at the Holtz hillslope experiment. B corresponds to examples at the catena of the plot experiments. Gravel content was classified in low (0), medium (1), high (2) and deposit layer with very few soil material (3). Core depth is the maximum drilling depth restricted by large stones or bedrock.

3.2 Plot experiments: Preferential bypassing to the deposit layer

Figure 3 shows the results of the plot-scale tracer experiments. Bromide recovery is given as recovered mass from the gridded

10 samples taken from the excavation face. Since the volume of the drilled core samples was larger, the values of the excavation face samples are scaled to the core sample volume for comparability. All plots suggest a relatively strong reaction in the depth of approximately 0.6 m. This depth correlates with the upper boundary of the first layer of periglacial deposits found in core B7 and in the excavated soil profiles. There the absence of developed soil material impedes water retention and allowed only disturbed sampling. This reaction is contrasted by low signals in shallower depth. Even plot XI, where only 30 mm were

15 applied, shows the same pattern with a clear breakthrough to the deposit layer.

At plot X we found stronger interaction with the soil matrix, which leads to a higher recovery coefficient (RC). Generally, the recovery is very low and even decreases when including the core samples. This points out that the sampling of only 0.5% of the affected soil volume cannot fully represent the highly heterogeneous distribution of irrigation water and that even this highly resolved sampling does not comprise the full picture.

5   The Brilliant Blue dye stains and the recorded soil moisture dynamics reflect a similar infiltration pattern. Especially at plot X and XII a relatively quick and strong reaction in $0.6\,m$ to $0.8\,m$ depth exceeds soil moisture changes in shallower layers. Stained patches in the deposit layer have been found in all plots and even several meters downhill the irrigation spot.

     Figures 4A to 4C show the depth profile of irrigation water as portion of total water content, calculated from the deviation in $\delta^2 H$ concentration between reference and $2h$ past irrigation core samples. The results are also compared to the Bromide

10   concentrations in the soil water phase of the same samples, showing slight correlation. However, the values are rather noisy due to low difference of the isotopic composition of the soil water and the not-enriched irrigation water. Figure 4D-E highlights the very weak soil moisture signal and low deviation between the respective soil cores close to the method's precision. Especially interpretation of the peak in about $0.5\,m$ depth and signals below may be erroneous, because the signature of the reference core coincides with the irrigation water there.

15   Although time-lapse GPR can only be used as qualitative information, it clarifies the ambiguity of the quantitative data in the context of spatial heterogeneity as it provides the spatial reference in two and three dimensions. In Figures 5 and 6, we present results of the 3D time-lapse GPR. The structural similarity attribute calculated between the data cubes at the respective acquisition time to the pre-irrigation one are plotted as mean over depth within three horizontal layers (top, mid, low) of $20\,ns$. High values refer to high similarity between the individual time steps, whereas low values can be associated with changes in

20   the data caused by a variation in the GPR velocity and therefore changes in subsurface water content. The recorded radargrams of a downslope transect are given in the lower row for the three acquisition times (0h, 1h, 20h). Due to the complex reflection energy patterns it is not suitable to trace individual reflectors. This prevents a quantitative interpretation as show by Allroggen et al. (2015b). However, by looking at the identified patches of low similarity underneath the infiltration area (blue), it is noteworthy that the irrigation water quickly spreads vertically during the irrigation experiment and follows a more lateral

25   trajectory afterwards. The results at plot X (not shown), where the measurement took slightly longer to accomplish, suggest that the lateral shift is actually taking place within the first hours after the end of irrigation.

3.3 Hillslope experiment: Discretely connected but leaky structures

Prior to the experiment the 3D GPR survey was conducted to explore potential subsurface flow structures. Figure 7 presents the semblance attribute (gray) and depth (yellow-red) of the picked GPR horizons. The identified patchy structures are mostly

30   located in about $1.5\,m$ depth which is in accordance with the soil cores (Figure 2, T1..T12). Especially T7 suggested an impermeable layer just below that depth.

     In addition Figure 7 also shows the observed hillslope response to the irrigation as presented in more detail by Angermann et al. (2016, this issue). Purple dots mark the position of the TDR profiles with the overall strength of their reaction indicated

by their respective size. Cyan dots mark the positions of the piezometers. At the GPR transect lines the overall lateral marginal distribution of the observed structural similarity attribute highlights areas with significant responses.

The results of the hillslope-scale irrigation experiment can be distinguished into the core area observations and observations at the downhill monitoring area, including TDR profiles as well as 2D GPR transects.

The soil moisture reaction at the core area is very much in line with the findings from the plot-scale experiments. Both experiments show a quick and clear reaction in greater depth, even before the intermediate layers respond. While the patterns are similar, the signal is stronger during the hillslope-scale experiment, which is due to the higher irrigation amount and duration. Within the margins of local heterogeneity and representativity of the TDR profiles this holds true for all four core area profiles. The downhill profiles, however, show a more divers reaction. This is exemplarily shown in Figure 8, where we present the change in soil moisture in TDR 2, 8, 9 and 11 referenced to the first record and attributed to irrigation water.

Close to the rain shield in TDR 3, 9 and 10 the profiles react very similarly to the patterns at the core area in distinct depth levels. This signal is somewhat conveyed but dampened and distorted to the next set of profiles (4, 11, 12). While the reaction is more and more limited to single depth levels and thus pointing to discrete connected flow paths, it remains rather ambiguous to determine their lateral connection. Moreover, the signal at the profiles varies strongly, which indicates once more that even the dense network of TDR profiles barely resolves the heterogeneous subsurface structures.

This is underpinned further by the observations in the piezometers and the isotopic composition of soil water in three successive soil cores, the irrigation water, and the preceding event water. Figure 9 presents the δ^2H data. It is noteworthy that only piezometer B at the core area gained sufficient water to be sampled more than once by very few mL. This very low reaction in comparison to the quick and strong soil moisture increase at all TDR profiles at the core area and in contrast to almost no signal in the other piezometers corroborates the finding that discrete structures govern the redistribution of the infiltration water. Although none of the irrigation water was specifically marked by isotopic enrichment, one can clearly identify that the water in piezometer B successively aligns with the signal of the soil water in the lower depth levels while deviating from the irrigation and storm event water values. Piezometer A and C match the signal of the irrigation water, while piezometer G and H can be very much attributed to the natural rain event.

Generally, the soil cores show no clear reaction to the irrigation. A more clear interpretation is inhibited by the very weak irrigation signal because the experiment was fed by stream water. Contrastingly, the preceding storm event appears to have more influence as visible by the topsoil signatures tending to less negative values. As the water collected in the downhill piezometers G and H matches the event signature the storm may have acted as primer for connectivity.

The four successive GPR transects across the downhill monitoring area provide further information on hillsope-scale flow patterns and boundary fluxes. Figure 10 comprises the observed reactions by presenting time-lapse structural similarity attribute referenced to the last measurement about 24 h after the end of the irrigation for exemplary times at transects 1 to 3. Moreover, the standard deviation of the attribute over time is used to identify regions of preferential flow using the same threshold again. The data corroborate that flow takes place in distinct structures and that they are heterogeneously distributed in the hillslope. Based on the discrimination between event water (green) and irrigation water (blue) further interpretation of the hillslope reaction becomes apparent: Flow structures are persistent and connected. Our irrigation triggered mostly different structures

Hydrology and
Earth System
Sciences

Open Access

Discussions

EGU

than the natural rainfall event. The impulse decays strongly with distance to the core area. Note that the last recorded difference $18\,h$ to $24\,h$ after irrigation start (not shown) exhibits high similarity in all profiles. The mean of the attribute is between 0.93 and 0.96, the median between 0.96 and 0.98 and standard deviation between 0.076 and 0.048 for GPR transect 1 and 3 respectively. The system appears to have reached a steady state without much further change in soil moisture.

5   The patchy structures at the transects highlight the distributed nature of preferential flow paths. As the signal observed in transect 1 does not simply propagate further downslope, the flow paths must be tortuous and leaky. Hence a direct connection between the four profiles in downhill direction is not feasible. Although some areas of the profiles exert a higher density of reacting flow paths than others, no such patterns could be specified throughout the hillslope. Given the absence of a clear subsurface reflector, which could mark a bedrock interface, it is not surprising that the piezometers did not react as intended.

10   This setting also underlines why the observed reactions in the TDR profiles are that heterogeneous.

Hydrology and
Earth System
Sciences
Discussions

Open Access

EGU
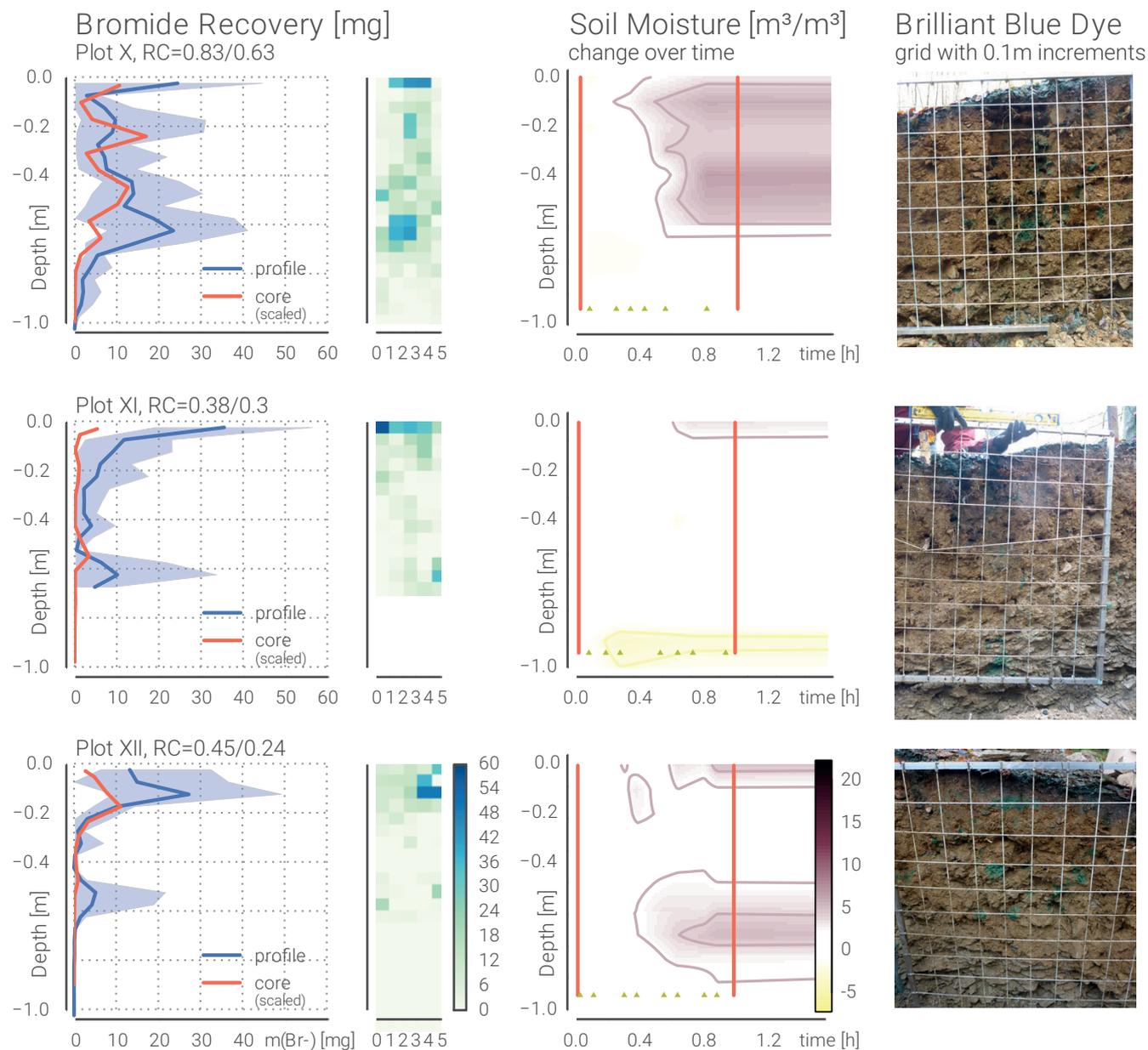
Figure 3. Results from plot-scale irrigation experiments with 50 mm, 30 mm and 50 mm spray irrigation for 1 h. Left: Recovered Bromide mass profiles and grids (5x5cm). Blue line as mean and shaded area between min/max for each depth of the sampling grid. Recovery coefficient (RC) calculated for the profile samples (first value) and the profile and core samples (second value). Center: Observed soil moisture change referenced to the first measurement shortly before onset of the irrigation. Individual measurements marked with triangles. Right: Photo with Brilliant Blue stains of excavation face on which the grid sampling took place.
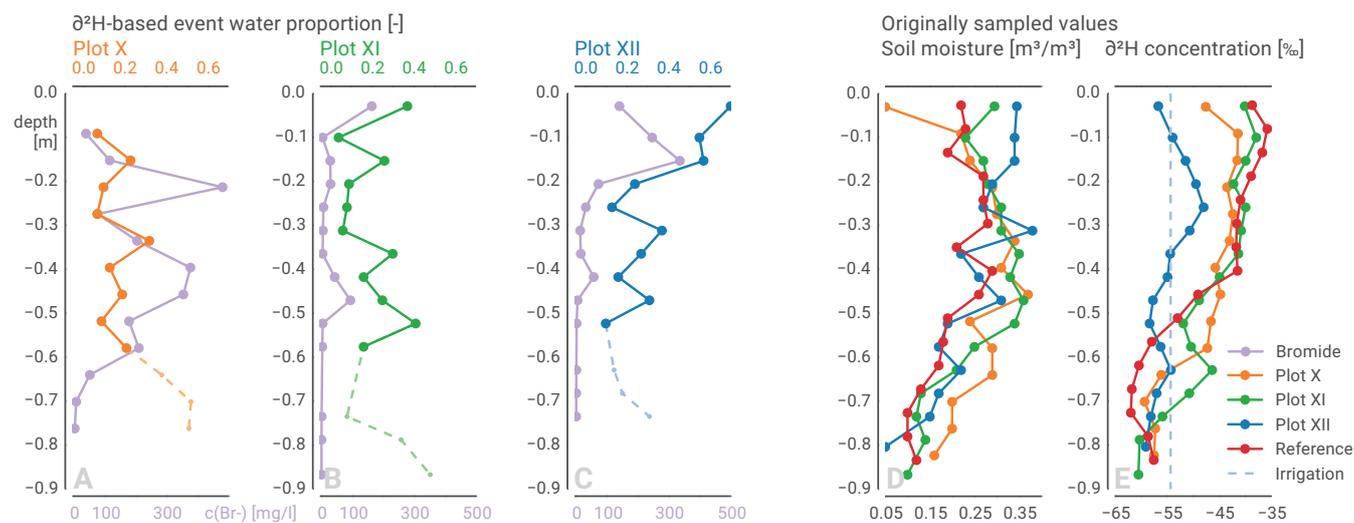
Figure 4. Plot-scale irrigation experiments. Proportion of event water derived from deviations in concentration of Deuterium and Bromide in soil water of sampled cores to reference (A-C). Absolute measured soil water content (D). Deuterium concentration in samples and signature of irrigation water (E). Note that the δ^2H concentration profiles and the signature of the irrigation water show low deviation and even coincide in $0.5\,\text{m}$ depth. Thus the interpretation needs precaution, especially below that level (dashed lines A-C).
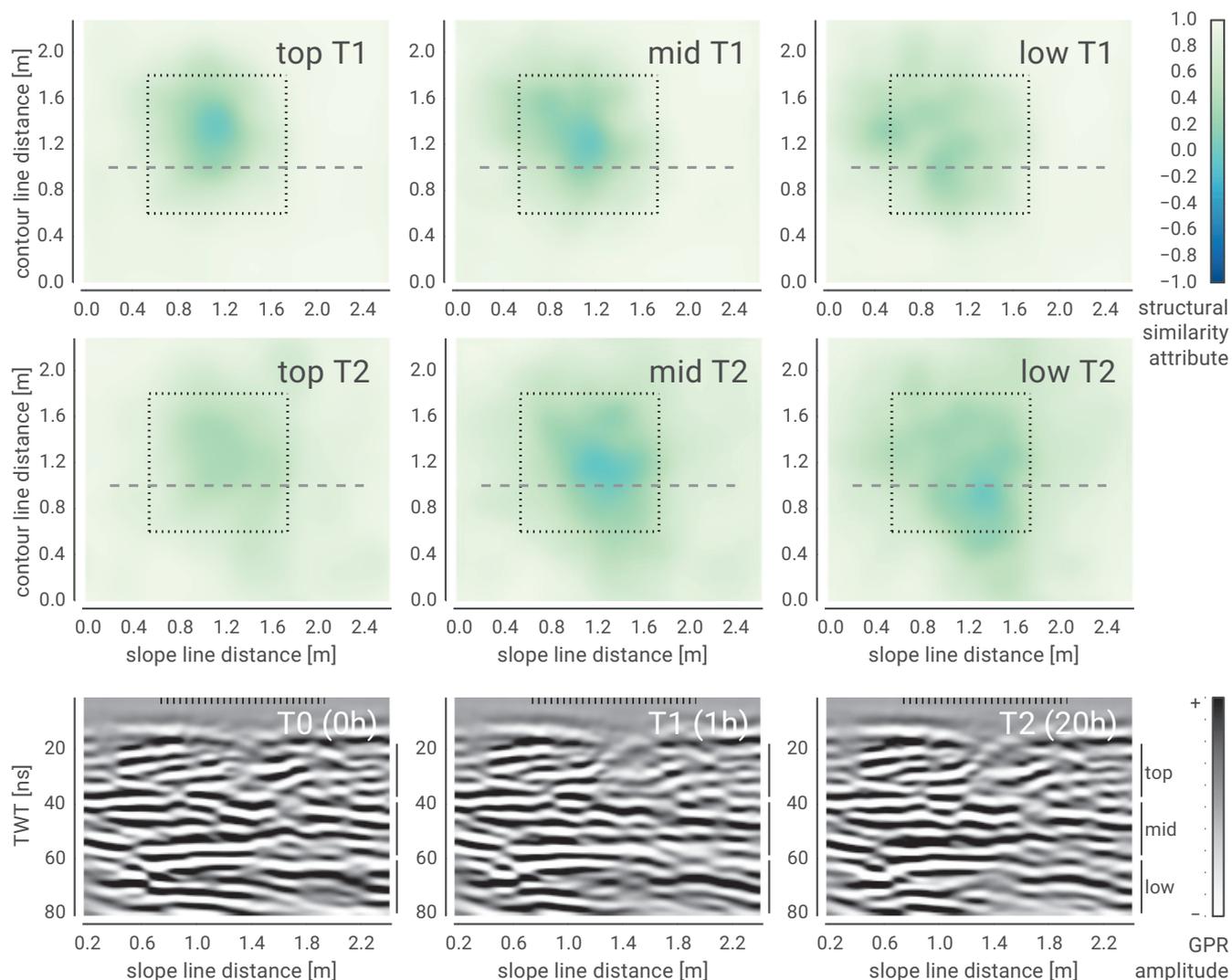
Figure 5. Time-lapse 3D GPR of irrigation experiment at plot XI. Structural similarity attribute in three different depth layers (top 20 ns to 40 ns, mid 40 ns to 60 ns, low 60 ns to 80 ns) between acquisition times T1-T0 (1) and T2-T0 (2). The original radargrams at the marked transect (grey dashed line) for the three acquisition times (T0, T1, T2) are given in the bottom row. The irrigation plot is marked by a black dashed box/line. Slope line distance increasing downslope.

Hydrology and
Earth System
Sciences

Open Access

Discussions

EGU
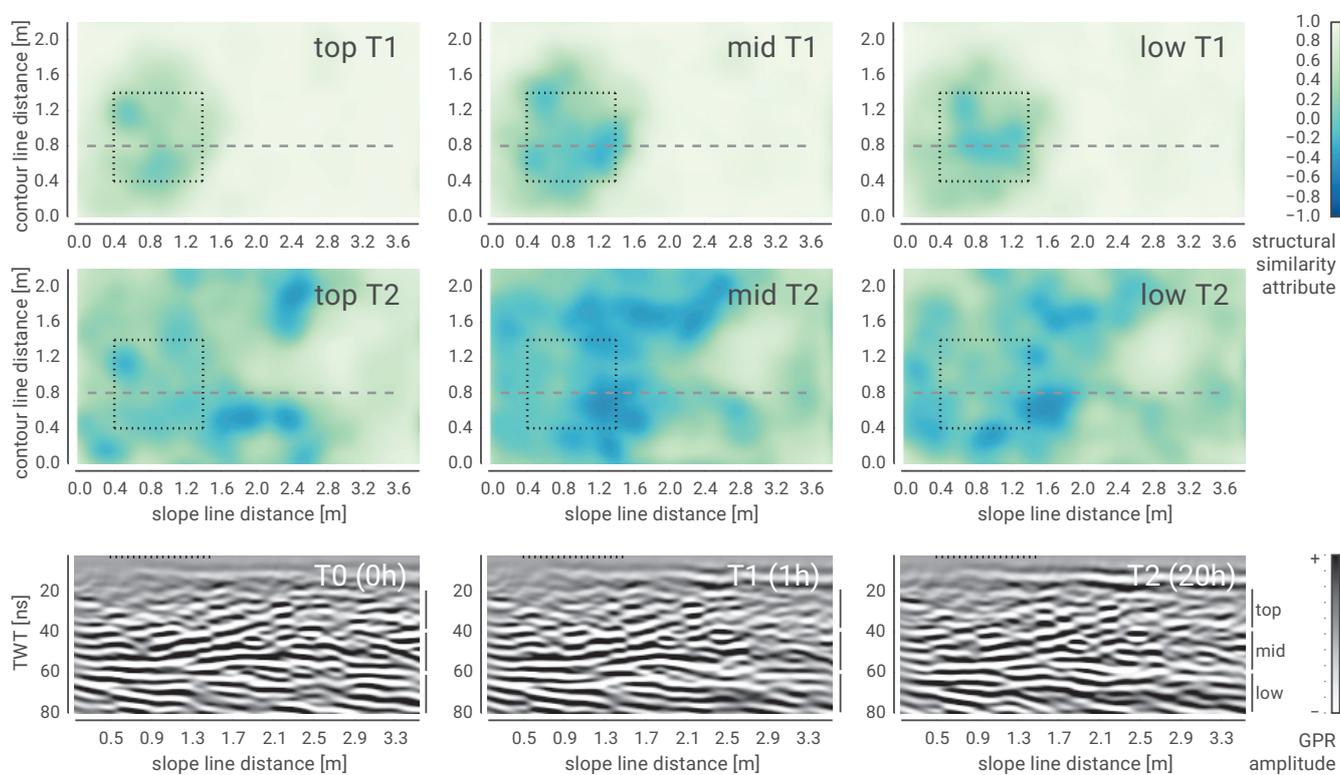
Figure 6. Time-lapse 3D GPR of irrigation experiment at plot XII. Structural similarity attribute in three different depth layers (top 20 ns to 40 ns, mid 40 ns to 60 ns, low 60 ns to 80 ns) between acquisitions T1-T0 (1) and T2-T0 (2). The original radargrams at the marked transect (grey dashed line) for the three acquisition times (T0, T1, T2) are given in the bottom row. The irrigation plot is marked by a black dashed box/line. Slope line distance increasing downslope.
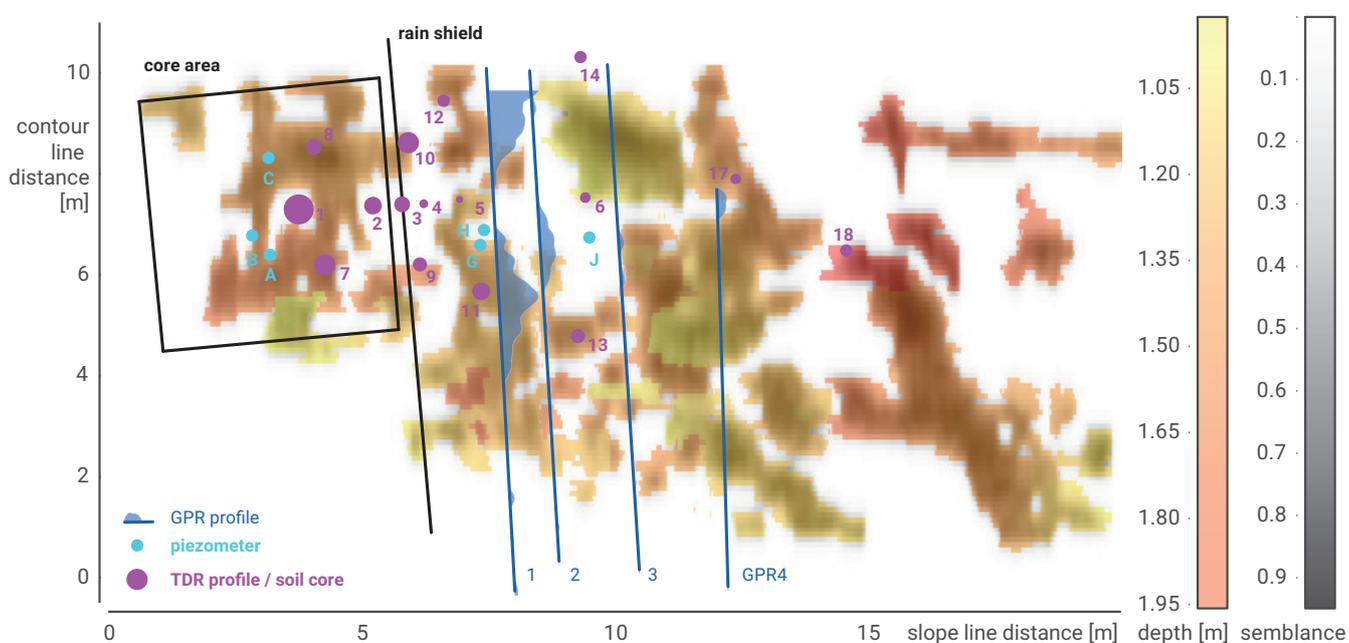
Figure 7. Potential subsurface structures from 3D GPR survey and setup of hillslope experiment. Structure identification guided by the dip corrected semblance attribute. Depth estimated based on mean measured effective radar velocity in soil of $0.07\,\mathrm{m\,ns^{-1}}$.

Summary of the hillslope experiment given by locations of TDR profile tubes (purple, also location of respective soil cores in Figure 2), GPR transects (blue) and piezometers (cyan). Dot size of TDR scaled to maximum of observed change in soil moisture. Along GPR transects lateral marginals of the structural similarity attribute as proxy for recorded advection.
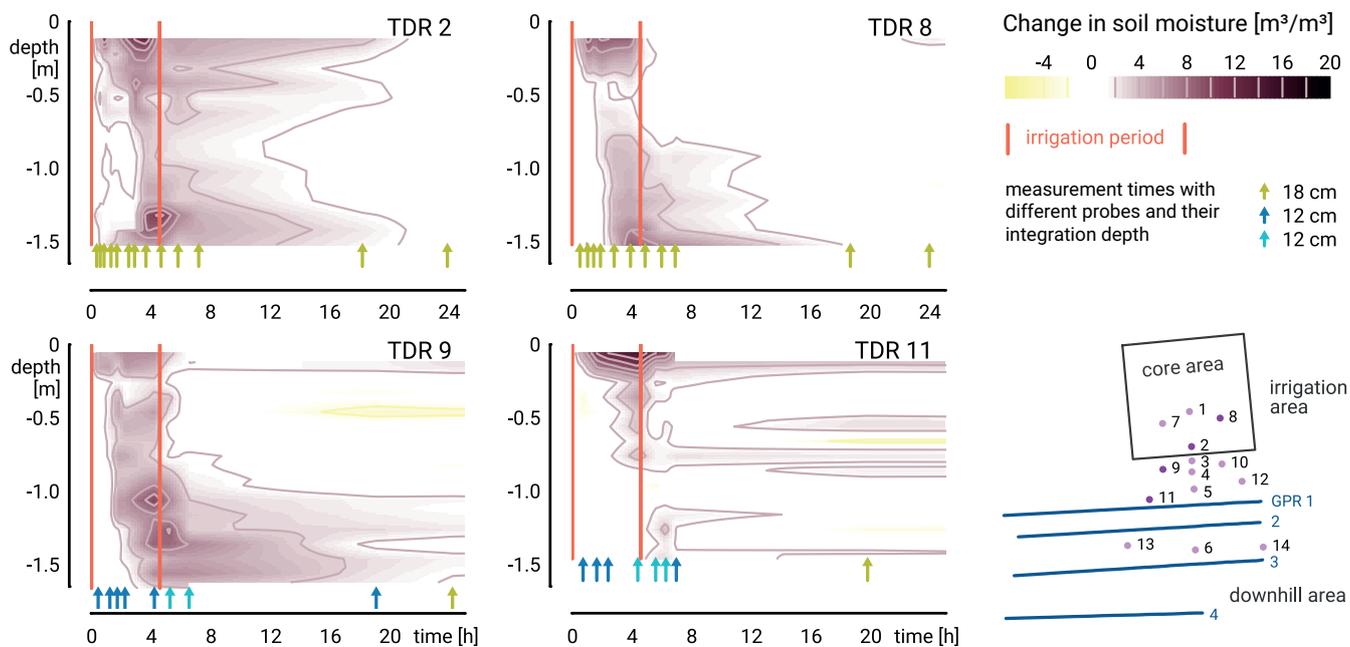
Figure 8. Development of soil moisture in TDR profiles during and after hillslope irrigation experiment. Exemplary transect with changes referenced to pre-irrigation conditions and attributed to irrigation water. Time is given in [h] after irrigation start. Individual measurements and probe reference marked with triangles. More data and explanation in Angermann et al. (2016), this issue.

Hydrology and
Earth System
Sciences

Open Access

EGU

Discussions
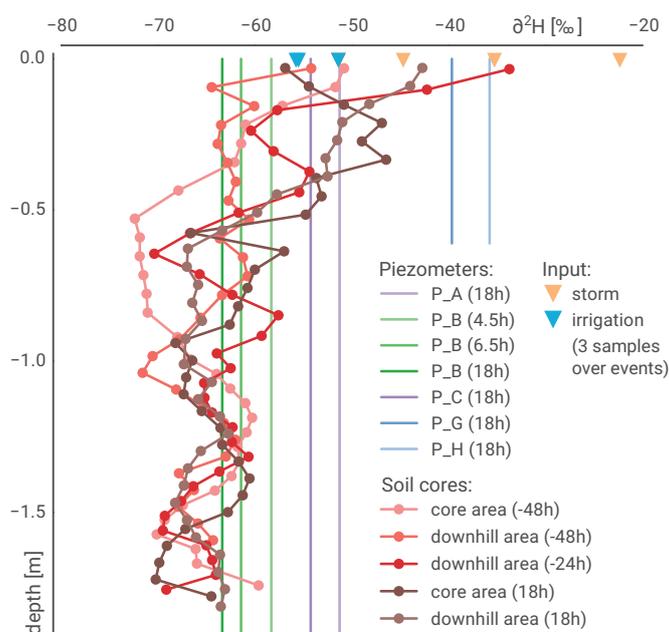
Figure 9. Deuterium composition (δ^2H) in soil core profiles and piezometer water samples. Times given relative to irrigation onset June 21, 5pm. Soil cores were taken before, in between and after the natural rain event and the irrigation experiment. Except for piezometer B, all piezometer samples are single snapshots in time, taken the day after the experiment.
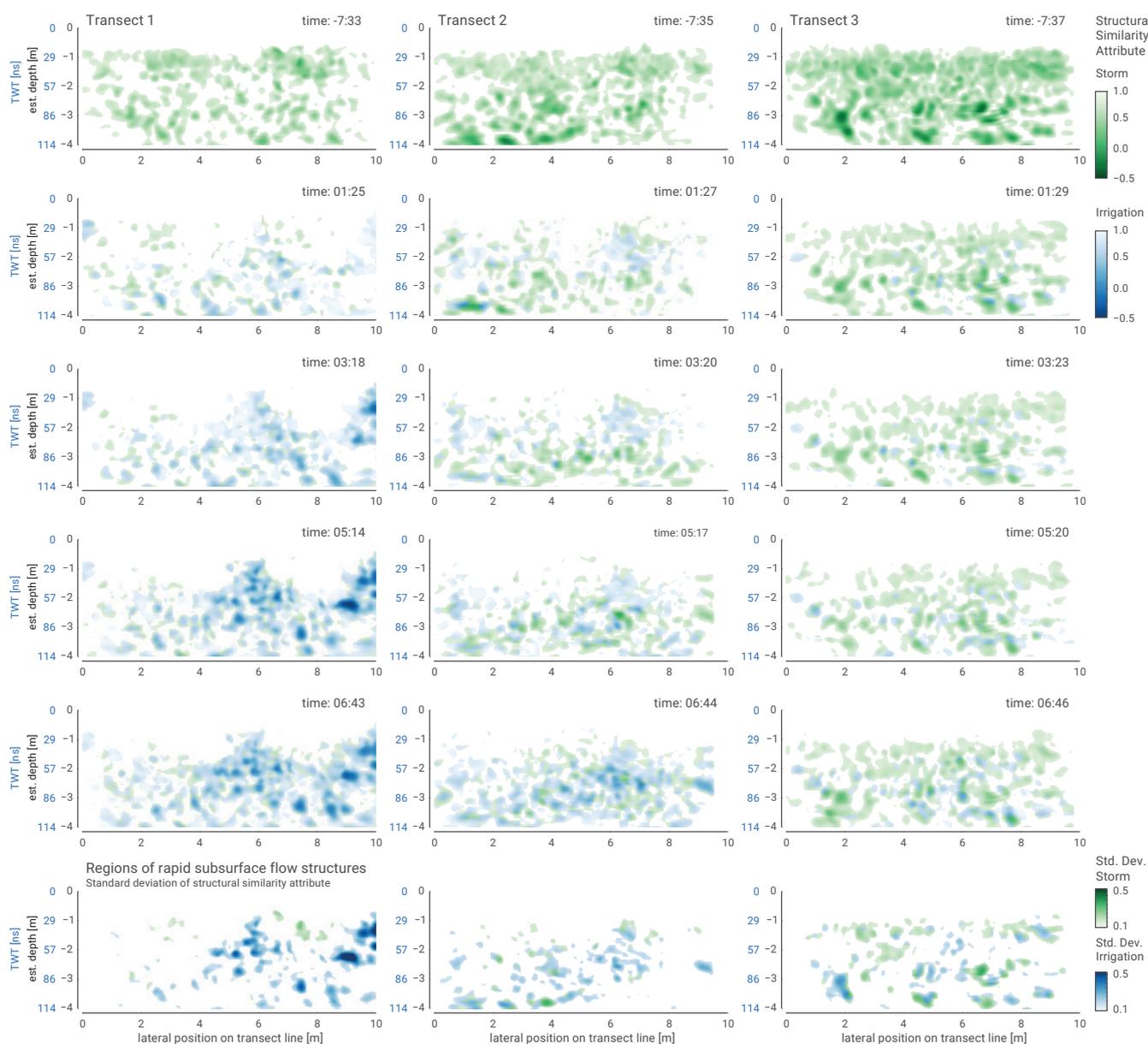
Figure 10. Structural similarity attribute in time-lapse 2D GPR transects. Blue: irrigation event water, Green: Storm event water. Columns: time series in one transect, Rows: different transects at the same time. Bottom row: Identified regions of rapid subsurface flow based on the standard deviation of all structural similarity attributes at one transect over time.

Notice: The structural similarity attribute calculates similarity between the radargram at the respective time to the last record 24 h past irrigation. A threshold or 0.15 is applied to ientify significant changes. It is a qualitative measure based on the assumption that the last record is in steady state and that all differences are induced by soil water redistribution.

4 Discussion

4.1 Process interpretation

4.1.1 Preferential flow at the plot- and hillslope-scale

The plot-scale tracer data confirm the existence of preferential flow and yield insight in its spatial characteristics. Preferential
flow paths are found to be at a scale of few mm and patterns are patchy and disconnected. Dye stains indicate diffusive
interaction with the surrounding matrix as result of respective interface surfaces, contact times, conductivity and/or supply
rates. Although it remains unclear which of the process dominates the exchange, it is evident that large parts of the soil are
bypassed. Even in the top soil below the litter layer only 12% of the horizontal outcrops are stained with Brilliant Blue.

Cracks, root channels and geogene structures govern rapid vertical redistribution at rates well above diffusive velocities.
From the presented experiments and as addressed in the first part of this study (Angermann et al., 2016, this issue) the advective
flow ranges at $10^{-3}\,\mathrm{m\,s^{-1}}$ to $10^{-4}\,\mathrm{m\,s^{-1}}$. Capillary driven diffusive flow alone is also not capable of producing the observed
patterns. Nevertheless diffusive processes play an important role with regard to the interaction between preferential flow paths
and the matrix. This finding contradicts the common assumption of separated and continuous domains of macropores and
matrix along a hillslope (Jury and Roth, 1990). At the same time, multi-porosity approaches will be challenged to define the
observed macropore-matrix exchange.

In addition to the fast vertical redistribution identified at the plot-scale, a lateral component is found in and above periglacial
deposit layers. At the hillsope-scale this appears as central control and exhibits itself as distorted leaky structure in which the
gravity driven advective flow field develops and quickly decays once the supply rate does not sustain it. The leaked water feeds
further percolation.

The processes together with the characteristics and extent of the geogene structures suggest that those observations are also
relevant at the larger scales. Lateral preferential flow paths potentially create connectivity across hillslopes, while macropore-
matrix interaction, vertical and diffusive flow processes control retardation and dissipation of the rainfall signals. At larger
scales this is found as multi-modal transit time distributions and has been investigated in other studies (e.g. Onda et al., 2001;
Wienhöfer et al., 2009). The specific temporal dynamics of the presented experiments are discussed by Angermann et al. (2016,
this issue).

4.1.2 Heterogeneity

The plot irrigation experiments point out that local measurements of hydrological properties necessarily could not step beyond
heterogeneity. The water quickly percolates in discrete structures and bypasses large proportions of the less conductive soil
matrix. Low recovery coefficients and the high variability within the excavation samples show, that point measurements are
barely representative even at the scale of few cm when the system is not close to local thermodynamic equilibrium.

Accordingly, the patchy patterns revealed by the time-lapse GPR measurements highlight the distributed nature of prefer-
ential flow paths. At the plot scale initially vertically funneled water is further laterally redistributed. This is seen as highly

patchy structure with most changes in the radar data cube outside the irrigation plot itself when sufficient irrigation input is supplied (compare Figure 5 and 6). At the larger scale this picture is retained by the diverse reaction at the TDR profiles and the lacking signal in the piezometers. It is further refined by 2D time-lapse GPR highlighting discrete flow paths. The lack of a clear connection between the individual GPR transects suggests that flow paths are tortuous and ephemerally connected. An

5   establishment of a groundwater table or discrete conductive layer was not observed.

4.1.3   Refinement of the perceptual model of the Colpach basin

With regard to the main characteristics of storage and drainage in the Colpach basin the findings of van den Bos et al. (2006) and Wrede et al. (2015) can be refined to a more discrete perception of the plot-scale reaction and hillslope architecture. The young soils exhibit silty characteristics with generally moderate retention capacity. They are interspersed with a network of

10   preferential flow paths which enable a quick funneled connection to the deposit layers in greater depth. There predominantly lateral redistribution takes place. Depending on the flow rates in these voids, water is lost to further percolation to the fractured bedrock interface.

The flow paths cover the entire hillslope and facilitate high response velocities and quick connectivity of a large portion of mobile water. As such the dip angle of the slope and the tortuosity and topology of the subsurface flow network may be the

15   central site controls. This also explains differences in reaction between the hillslopes under study and plateau hill tops with low topographic gradient. The latter results in more deep percolation and thus contribution to the fill and spill mechanisms (Tromp-van Meerveld and McDonnell, 2006) at the bedrock interface.

4.2   Methodological discussion

4.2.1   Local exploration

20   In the face of the explored rapid subsurface flow structures, it is apparent that the initially introduced exploration strategy based on distributed measurements of infiltration capacity, saturated hydraulic conductivity and soil water retention properties deserves revision. While the overall mean characteristics may be described well with this data basis, it is insufficient to relate the findings to specific compartments in the heterogeneous domain. The relatively large spatial footprint of a single sample or measurement as well as its imprecise localization prohibit to unravel the different spectra of advective and diffusive flow

25   processes. With this, the local differences in macropore-matrix exchange and the divers funneling in the macroporous network reduce to sub-scale noise in the data.

The key to the identification of structured subsurface flow paths was to intensively monitor the system under driven conditions in irrigation experiments, but also to employ a continuous imaging technique. To improve hydrological exploration methodology a revision should target more specifically on the different process domains like infiltration, redistribution and

30   funneling, macropore capacity, matrix conductivity, and macropore-matrix interaction. As such a hypothesis-driven study of the interplay of the system's compartments and the driving gradients can be identified and linked back to their spatial distri-

bution. With regard to the soil water retention characteristics the influence of voids and gravel demands for a more thorough analysis.

4.2.2 TDR profiles

The size of preferential flow structures is in the range of 10^{-3} m to 10^{-2} m. However, soil moisture measurements could only

5 be realized in the desired density and continuity with a technique integrating over 1.2×10^{-1} m and 1.8×10^{-1} m in depth. We could slightly enhance the resolution with overlapping the respective increments. While large integration volumes are preferable for representativity of such a measurement, it also smoothes out the effect of preferential flow in a single record. In addition to the issue of the relatively large depth increment compared to the much smaller preferential flow structures, the penetration depth of the TDR signal into the soil is depending on the soil moisture distribution, too. Hence, we may likely

10 underestimate the absolute changes in soil water content inside specific flow paths.

The employed resampling of the TDR measurements to a regular grid in time and space was selected to avoid undesired smoothing. Because soil moisture is not continuous at interfaces, interpolation smoothes out important information about sharp gradients. With regard to the localized flow structures larger interpolation would quickly inhibit their detection. Lateral interpolation between different TDR profiles over distances of about 1 m is thus unfeasible. Furthermore, a connective continuum

15 cannot be assumed over larger distances in the given young soils.

Moreover, the quantification of advective water from the recorded changes in soil moisture has proven not feasible. Given the insight of the discretely structured flow domain and the high velocities identified earlier (Angermann et al., 2016, this issue), the soil moisture measurements leave us with many questions. It is noteworthy that they exhibit a conceptual bias towards the diffusive fraction of the soil water. As for the local exploration, a precise location of such monitoring at specific points in the

20 domain (e.g. directly at responsive structures and at less reactive places) may enhance the interpretability of the monitoring data.

4.2.3 Tracer application and stable isotopes at the plot scale

Application of tracers at the plot scale was the basis to identify dominant flow processes and highly reduced the ambiguity of the point exploration. With recovered Brilliant Blue stains even far from the irrigation area (4 m downslope, 1 m deep) the role

25 of rapid flow is apparent. The analyzed concentration profiles of Br^- add quantitative description of the advective flow field.

With attention to the structured soil domain and the results from the time-lapse GPR, the Br^- tracer results appear less representative. Although Br^- measurements are quantitative in general, they are insufficient to really close the mass balance due to a lack of information about the whole system, structured components and boundary fluxes. Similar to soil moisture monitoring, tracer data in the soil water phase also requires a sample size which integrates a non-determined fraction of

30 structures and soil matrix. The total sampled volume accounts for less than 0.5% of the affected soil. With adding the drilled core samples to the set, recovery coefficients decline for all plots. Hence we have not reached an ergodic sampling. Therefore, the quantitative results need to consider large bands of uncertainty.

In line with the findings of Klaus et al. (2013) the isotopic signal of non-enriched water required strong assumptions for its interpretation. In our case this specifically applies to the plot scale core samples where we calculated the difference to the pre-experiment core regardless the fact, that soil water and irrigation water deviated only slightly ($\geq 15 \permil$) and even had the same values in $0.5\,\mathrm{m}$ depth. Moreover, the reference core was required to be at a different location. Hence flow paths and thus

5 the initial isotope profile are not necessarily the same as at the respective plots. However, as assumably ideal tracer the stable isotope data allowed for an additional and coherent measurement. With respect to the overall findings of rapid flow in discrete structures the assumption is justified.

Despite all uncertainty, the biggest strength of the plot experiments is the spatially distributed observation of the result from a controlled process. What is lacking is a better resolution in time and a more thorough image of the subsurface.

10 ### 4.2.4 GPR survey and time-lapse application

Inferring subsurface structures from radar data without any continuously identifiable reflector in a complex setting has been proven as fundamental challenge. For the interpretation of the GPR survey we use the semblance attribute which highlights spatially similar areas within the GPR data. However, areas of high structural continuity or areas of complex reflection patterns are not necessarily connected to subsurface flow processes. Hence the limitations of this approach simply arise from the missing

15 contrast between flow structures and the heterogeneity at the site.

In comparison to the reaction of some structures to irrigation (figure 9) the picked horizons are very complex and their reference as hydrologically relevant layers appears ambiguous. Contrastingly, direct comparison of repetitive acquisitions of the same transect through the structural similarity attribute (Allroggen and Tronicke, 2016) images areas of activated flow paths very well.

20 In this setting, differences between successive radargrams (as used for the structural similarity attribute) highlight specific areas of low structural similarity, which can be interpreted to be connected to subsurface flow. The comparison of radargrams in time needs further attention: In other time-lapse GPR applications for soil water dynamics in structured domains (Truss et al., 2007; Haarder et al., 2011; Allroggen et al., 2015b; Klenk et al., 2015) analysis is guided by reference to a reflector and its apparent displacement can be used to calculate changes in soil moisture. Alternatively, a wetting front could generate a

25 reflector (Léger et al., 2014). In our case none of these existed. Moreover we assume that changes in soil moisture in discrete structures in an upper layer do not effect the overall GPR velocity to detect structures below. Thus the demand on the precision of the repeated acquisition with spatial determination and antenna contact to the ground are very high and are assumed to be nearly perfect within our experiments. The missing reflector also inhibited any estimation of quantitative values. Further, the referenced depths in figure 10 are only estimates based on a measured mean GPR velocity which can also vary depending on

30 the initial conditions.

The highlighted assumptions clearly frame the limits of the technique. Under field conditions precision is limited due to numerous effects like micro-topography, top-soil conditions, signal attenuation and even weather. The overall sensitivity of the approach can be judged from the structural similarity attribute of the last pairs of records with a mean of the temporal standard deviations of the attribute of 0.061 as shown in figure 11. This also implies that weak reactions and local effects must not be

over interpreted. Hence, the introduced threshold of 0.15 for irrigation signal detection appears to be a reasonable choice for qualitative interpretation.
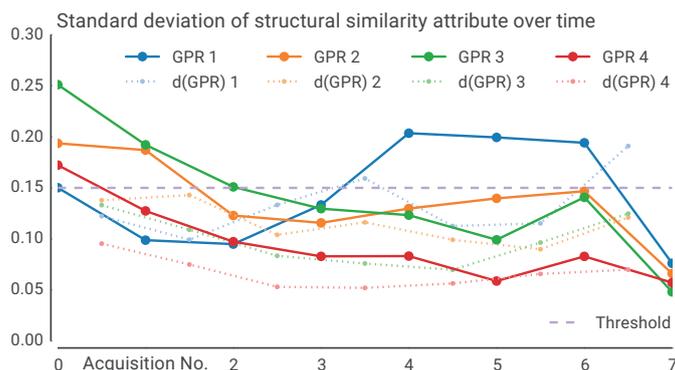
Figure 11. Standard deviation of structural similarity attribute at the different transects over time (solid lines) and standard deviation of the differences of two successive attribute distributions (dotted lines).

Another limit is the interpretability of changes in the radargrams, as water can have different effects under different situations. A wetted well-defined surface may quickly become a reflector which is easy to detect. However, tortuous flow paths may not

5 be as ideal and small structures might be well below the limits of detectability in the complex reflection pattern. As such the structural similarity attribute can only detect zones of strong changes which can be induced by many lumped small structures, one big flow path, or even a favorably oriented stone which gets wetted.

Nevertheless and with respect to the employed local measurements, time-lapse GPR is an insightful technique with many advantages: Especially with regard to tracer applications time-lapse GPR can add spatio-temporal information to excavated dye

10 patterns or sampled salt tracer concentration, which only allow for a single retrospective measurement. Time-lapse GPR also exhibits the potential to overcome some of the spatial restrictions of an excavation and partial sampling. Owing the fact that dye stains can only be used as indicators to trace activated flow paths, and that soil samples necessarily consist of a mixture of matrix and macropore, time-lapse GPR may also be developed to an alternative, non-invasive monitoring technique.

Concerning spatial and temporal resolution the experiments clearly depict that we operate at the limits of the requirements by

15 the structures and processes. Although higher radar frequencies could facilitate higher resolution of the flow structures it will also result in greater attenuation of the signal limiting penetration depth. Temporal resolution can especially be enhanced for the 2D time-lapse application at the cost of some of the downslope transects. Much more methodological progress is envisaged by a more specific combination of TDR and GPR techniques (e.g. Huisman et al., 2001) towards means to quantify GPR inferred changes in soil moisture. The challenge of *in situ* imaging of subsurface flow processes is thus still not fully solved by

20 time-lapse GPR alone but requires coherent embedding in an experimental setup that activates the structures and complements the imaging through accompanying techniques.

5 Conclusions

We have shown that rapid subsurface flow in the young soils on periglacial slope deposits takes place in specific structures which are connective along the hillslope. While these structures are very distinct and leading event water to bypass large proportions of the soil, especially horizontal structures are also tortuous and leaky, making it particularly difficult to reduce the system to a simple dual domain approximation. These findings complement the first part of the companion paper on the temporal perspective (Angermann et al., 2016, this issue). The large portion of mobile water is funneled in such structures at high response velocities even exceeding $10^{-3}\,\mathrm{m\,s^{-1}}$.

From a methodological perspective, we presented a multitude of possible approaches to hydrological system characterization from local exploration to plot- and hillslope irrigation experiments. Without information about the general setting any point measurement in the structured domain is rendered futile as its representativity and spatial reference remain unknown. As such it can only be attributed to local heterogeneity. Also a 3D GPR survey as spatially continuous exploration did not determine the network of subsurface flow structures.

The coherent combination of different methods to monitor driven cases when the structures are activated was key to reduce ambiguity of any single observation. The detection of fast and small-scale soil water dynamics was realized by non-invasive time-lapse GPR in multiple 2D transects and 3D data cubes. However, the fast and small-scale processes demand very high spatial and temporal resolution of the measurements which deserves further improvement.

Although the distributed data is of qualitative nature, it allows to set local quantitative measurements into perspective and to identify spatially persistent flow structures. Once we can combine the overall distribution through an imaging of the subsurface flow processes with continuous local quantitative measurements the system may be well-described. As such, this combination of driven cases, imaging techniques and quantitative measurements exhibits potential avenues for system characterization over excessive accumulation of point information. In combination with exploratory model applications this is envisaged to be employed as novel hydrological survey tool at the hillslope scale.

Hydrology and
Earth System
Sciences

Open Access

EGU

Discussions

Hydrology and
Earth System
Sciences

Discussions

EGU

Open Access

References

Allaire, S. E., Roulier, S., and Cessna, A. J.: Quantifying preferential flow in soils: A review of different techniques, JOURNAL OF HY-
DROLOGY, 378, 179–204, doi:10.1016/j.jhydrol.2009.08.013, 2009.

Allroggen, N. and Tronicke, J.: Attribute-based analysis of time-lapse ground-penetrating radar data, GEOPHYSICS, 81, H1–H8,
doi:10.1190/geo2015-0171.1, 2016.

Allroggen, N., Tronicke, J., Delock, M., and B o niger, U.: Topographic migration of 2D and 3D ground-penetrating radar data considering
variable velocities, NEAR SURFACE GEOPHYSICS, 13, 253–259, doi:10.3997/1873-0604.2014037, 2015a.

Allroggen, N., van Schaik, N. L. M. B., and Tronicke, J.: 4D ground-penetrating radar during a plot scale dye tracer experiment, JOURNAL
OF APPLIED GEOPHYSICS, 118, 139–144, doi:10.1016/j.jappgeo.2015.04.016, 2015b.

Amoozegar, A.: Comparison of the Glover Solution with the Simultaneous-Equations Approach for Measuring Hydraulic Conductivity,
SOIL SCIENCE SOCIETY OF AMERICA JOURNAL, 53, 1362, doi:10.2136/sssaj1989.03615995005300050010x, 1989.

Anderson, A. E., Weiler, M., Alila, Y., and Hudson, R. O.: Dye staining and excavation of a lateral preferential flow network, HYDROLOGY
AND EARTH SYSTEM SCIENCES, 13, 935–944, doi:10.5194/hess-13-935-2009, 2009.

Angermann, L., Jackisch, C., Allroggen, N., Sprenger, M., Zehe, E., Tronicke, J., Weiler, M., and Blume, T.: Experimental investigation
of rapid sub-surface flow: temporal dynamics and catchment-scale importance, HYDROLOGY AND EARTH SYSTEM SCIENCES,
submitted.

Beven, K. and Germann, P.: Macropores and water flow in soils, WATER RESOURCES RESEARCH, 18, 1311–1325,
doi:10.1029/WR018i005p01311, 1982.

Beven, K. and Germann, P.: Macropores and water flow in soils revisited, WATER RESOURCES RESEARCH, 49, 3071–3092,
doi:10.1002/wrcr.20156, 2013.

Birken, R. and Versteeg, R.: Use of four-dimensional ground penetrating radar and advanced visualization methods to determine subsurface
fluid migration, JOURNAL OF APPLIED GEOPHYSICS, 43, 215–226, doi:10.1016/S0926-9851(99)00060-9, 2000.

Blouin, M., Hodson, M. E., Delgado, E. A., Baker, G., Brussaard, L., Butt, K. R., Dai, J., Dendooven, L., Peres, G., Tondoh, J. E., Cluzeau,
D., and Brun, J. J.: A review of earthworm impact on soil function and ecosystem services, EUROPEAN JOURNAL OF SOIL SCIENCE,
64, 161–182, doi:10.1111/ejss.12025, 2013.

Blume, T. and van Meerveld, H. J. I.: From hillslope to stream: methods to investigate subsurface connectivity, WILEY INTERDISCI-
PLINARY REVIEWS: WATER, 2, 177–198, doi:10.1002/wat2.1071, 2015.

Fenicia, F., Kavetski, D., Savenije, H. H. G., Clark, M. P., Schoups, G., Pfister, L., and Freer, J.: Catchment properties, function, and
conceptual model representation: is there a correspondence?, HYDROLOGICAL PROCESSES, 28, 2451–2467, doi:10.1002/hyp.9726,
2014.

Flury, M., Flühler, H., Jury, W. A., and Leuenberger, J.: Susceptibility of soils to preferential flow of water: A field study, WATER RE-
SOURCES RESEARCH, 30, 1945–1954, doi:10.1029/94WR00871, 1994.

Gerke, H. H.: Preferential flow descriptions for structured soils, JOURNAL OF PLANT NUTRITION AND SOIL SCIENCE, 169, 382–400,
doi:10.1002/jpln.200521955, 2006.

Germann, P. F.: Preferential Flow, Geographica Bernensia, Institute of Geography, University of Bern, Bern, 2014.

Graham, C. B., Woods, R. A., and McDonnell, J. J.: Hillslope threshold response to rainfall: (1) A field based forensic approach, JOURNAL
OF HYDROLOGY, 393, 65–76, doi:10.1016/j.jhydrol.2009.12.015, 2010.

Guo, L., Chen, J., and Lin, H.: Subsurface lateral preferential flow network revealed by time-lapse ground-penetrating radar in a hillslope, WATER RESOURCES RESEARCH, 50, 9127–9147, doi:10.1002/2013WR014603, 2014.

Gupta, H., Clark, M. P., Vrugt, J. A., Abramowitz, G., and Ye, M.: Towards a Comprehensive Assessment of Model Structural Adequacy, WATER RESOURCES RESEARCH, 48, 1–40, doi:10.1029/2011WR011044, 2012.

5 Haarder, E. B., Looms, M. C., Jensen, K. H., and Nielsen, L.: Visualizing unsaturated flow phenomena using high-resolution reflection ground penetrating radar, VADOSE ZONE JOURNAL, 10, 84–97, doi:10.2136/vzj2009.0188, 2011.

Heller, K.: Einfluss periglazialer Deckschichten auf die oberflächennahen Fließwege am Hang - eine Prozessstudie im Osterzgebirge, Sachsen, Ph.D. thesis, Technical University Dresden, 2012.

Holländer, H. M., Bormann, H., Blume, T., Buytaert, W., Chirico, G. B., Exbrayat, J. F., Gustafsson, D., Hölzel, H., Krausse, T., Kraft, P., 10 Stoll, S., Bloschl, G., and Flühler, H.: Impact of modellers' decisions on hydrological a priori predictions, HYDROLOGY AND EARTH SYSTEM SCIENCES, 18, 2065–2085, doi:10.5194/hess-18-2065-2014, 2014.

Huisman, J. A., Sperl, C., Bouten, W., and Verstraten, J. M.: Soil water content measurements at different scales: accuracy of time domain reflectometry and ground-penetrating radar, JOURNAL OF HYDROLOGY, 245, 48–58, doi:10.1016/S0022-1694(01)00336-5, 2001.

Jarvis, N. J.: A review of non-equilibrium water flow and solute transport in soil macropores: principles, controlling factors and consequences 15 for water quality, EUROPEAN JOURNAL OF SOIL SCIENCE, 58, 523–546, doi:10.1111/j.1365-2389.2007.00915.x, 2007.

Juilleret, J., Iffly, J. F., Pfister, L., and Hissler, C.: Remarkable Pleistocene periglacial slope deposits in Luxembourg (Oesling): pedological implication and geosite potential, Bulletin de Société des Naturalistes Luxembourgeois, 2011.

Jury, W. A. and Roth, K.: Transfer functions and solute movement through soil, theory and applications, Birkhauser, Basel, 1990.

Kasteel, R., Vogel, H.-J., and Roth, K.: Effect of non-linear adsorption on the transport behaviour of Brilliant Blue in a field soil, EUROPEAN 20 JOURNAL OF SOIL SCIENCE, 53, 231–240, doi:10.1046/j.1365-2389.2002.00437.x, 2002.

Klaus, J. and Zehe, E.: Modelling rapid flow response of a tile-drained field site using a 2D physically based model: assessment of 'equifinal' model setups, HYDROLOGICAL PROCESSES, 24, 1595–1609, doi:10.1002/hyp.7687, 2010.

Klaus, J. and Zehe, E.: A novel explicit approach to model bromide and pesticide transport in connected soil structures, HYDROLOGY AND EARTH SYSTEM SCIENCES, 15, 2127–2144, doi:10.5194/hess-15-2127-2011, 2011.

25 Klaus, J., Zehe, E., Elsner, M., Külls, C., and McDonnell, J. J.: Macropore flow of old water revisited: experimental insights from a tile-drained hillslope, HYDROLOGY AND EARTH SYSTEM SCIENCES, 17, 103–118, doi:10.5194/hess-17-103-2013, 2013.

Klenk, P., Jaumann, S., and Roth, K.: Quantitative high-resolution observations of soil water dynamics in a complicated architecture using time-lapse ground-penetrating radar, HYDROLOGY AND EARTH SYSTEM SCIENCES, 19, 1125–1139, doi:10.5194/hess-19-1125-2015, 2015.

30 Léger, E., Saintenoy, A., and Coquet, Y.: Hydrodynamic parameters of a sandy soil determined by ground-penetrating radar inside a single ring infiltrometer, WATER RESOURCES RESEARCH, 50, 5459–5474, doi:10.1002/2013WR014226, 2014.

Marfurt, K. J., Kirlin, R. L., Farmer, S. L., and Bahorich, M. S.: 3-D seismic attributes using a semblance-based coherency algorithm, GEOPHYSICS, 63, 1150–1165, 1998.

McDonnell, J. J., Freer, J., Hooper, R., Kendall, C., Burns, D., Beven, K., and Peters, J.: New method developed for studying flow on 35 hillslopes, EOS, TRANSACTIONS AMERICAN GEOPHYSICAL UNION, 77, 465–472, doi:10.1029/96EO00306, 2011.

McGuire, K. J. and McDonnell, J. J.: Hydrological connectivity of hillslopes and streams: Characteristic time scales and nonlinearities, WATER RESOURCES RESEARCH, 46, W10543, doi:10.1029/2010WR009341, 2010.

Nadezhdina, N., David, T. S., David, J. S., Ferreira, M. I., Dohnal, M., Tesar, M., Gartner, K., Leitgeb, E., Nadezhdin, V., Cermak, J., Jimenez, M. S., and Morales, D.: Trees never rest: the multiple facets of hydraulic redistribution, ECOHYDROLOGY, 3, 431–444, doi:10.1002/eco.148, 2010.

Onda, Y., Komatsu, Y., Tsujimura, M., and Fujihara, J.-i.: The role of subsurface runoff through bedrock on storm flow generation, HYDRO-
5   LOGICAL PROCESSES, 15, 1693–1706, doi:10.1002/hyp.234, 2001.

Palm, J., van Schaik, N. L. M. B., and Schröder, B.: Modelling distribution patterns of anecic, epigeic and endogeic earthworms at catchment-scale in agro-ecosystems, PEDOBIOLOGIA, 56, 23–31, doi:10.1016/j.pedobi.2012.08.007, 2012.

Sander, T. and Gerke, H. H.: Modelling field-data of preferential flow in paddy soil induced by earthworm burrows, JOURNAL OF CON-TAMINANT HYDROLOGY, 104, 126–136, doi:10.1016/j.jconhyd.2008.11.003, 2009.

10 Schotanus, D., van der Ploeg, M. J., and van der Zee, S. E. A. T. M.: Quantifying heterogeneous transport of a tracer and a degradable contam-inant in the field, with snowmelt and irrigation, HYDROLOGY AND EARTH SYSTEM SCIENCES, 16, 2871–2882, doi:10.5194/hess-16-2871-2012, 2012.

Sprenger, M., Herbstritt, B., and Weiler, M.: Established methods and new opportunities for pore water stable isotope analysis, HYDRO-LOGICAL PROCESSES, 29, 5174–5192, doi:10.1002/hyp.10643, 2015a.

15 Sprenger, M., Volkmann, T. H. M., Blume, T., and Weiler, M.: Estimating flow and transport parameters in the unsaturated zone with pore water stable isotopes, HYDROLOGY AND EARTH SYSTEM SCIENCES, 19, 2617–2635, doi:10.5194/hess-19-2617-2015, 2015b.

Trinks, I., St u mpel, H., and Wachsmuth, D.: Monitoring water flow in the unsaturated zone using georadar, FIRST BREAK, 19, 679–684, 2001.

Tromp-van Meerveld, H. and McDonnell, J. J.: Threshold relations in subsurface stormflow: 2. The fill and spill hypothesis, WATER RE-
20 SOURCES RESEARCH, 42, W02 411, doi:10.1029/2004WR003800, 2006.

Tronicke, J. and Böniger, U.: GPR attribute analysis: There is more than amplitudes, FIRST BREAK, 31, 2013.

Truss, S., Grasmueck, M., Vega, S., and Viggiano, D. a.: Imaging rainfall drainage within the Miami oolitic limestone using high-resolution time-lapse ground-penetrating radar, WATER RESOURCES RESEARCH, 43, 1–15, doi:10.1029/2005WR004395, 2007.

Uhlenbrook, S.: Catchment hydrology - a science in which all processes are preferential, HYDROLOGICAL PROCESSES, 20, 3581–3585,
25 doi:10.1002/hyp.6564, 2006.

van den Bos, R., Hoffmann, L., Juilleret, J., Matgen, P., and Pfister, L.: Conceptual modelling of individual HRU's as a trade-off between bottom-up and top-down modelling, a case study, iemss.org, 2006.

van Meerveld, H. J., Seibert, J., and Peters, N. E.: Hillslope–riparian-stream connectivity and flow directions at the Panola Mountain Research Watershed, HYDROLOGICAL PROCESSES, 29, 3556–3574, doi:10.1002/hyp.10508, 2015.

30 van Schaik, L., Palm, J., Klaus, J., Zehe, E., and Schröder, B.: Linking spatial earthworm distribution to macropore numbers and hydrological effectiveness, ECOHYDROLOGY, 7, 401–408, doi:10.1002/eco.1358, 2014.

van Schaik, N. L. M. B.: Spatial variability of infiltration patterns related to site characteristics in a semi-arid watershed, CATENA, 78, 36–47, doi:10.1016/j.catena.2009.02.017, 2009.

Vogel, H.-J. and Roth, K.: Moving through scales of flow and transport in soil, JOURNAL OF HYDROLOGY, 272, 95–106,
35 doi:10.1016/S0022-1694(02)00257-3, 2003.

Vogel, H.-J., Cousin, I., Ippisch, O., and Bastian, P.: The dominant role of structure for solute transport in soil: experimental evidence and modelling of structure and transport in a field experiment, HYDROLOGY AND EARTH SYSTEM SCIENCES, 10, 495–506, doi:10.5194/hess-10-495-2006, 2006.

Hydrology and
Earth System
Sciences

Discussions

Open Access

EGU

Wassenaar, L. I., Hendry, M. J., Chostner, V. L., and Lis, G. P.: High Resolution Pore Water $\delta 2H$ and $\delta 18O$ Measurements by H2O (liquid) - H2O (vapor) Equilibration Laser Spectroscopy, ENVIRONMENTAL SCIENCE & TECHNOLOGY, 42, 9262–9267, doi:10.1021/es802065s, 2008.

Wienhöfer, J. and Zehe, E.: Predicting subsurface stormflow response of a forested hillslope – the role of connected flow paths, HYDROLOGY AND EARTH SYSTEM SCIENCES, 18, 121–138, doi:10.5194/hess-18-121-2014, 2014.

Wienhöfer, J., Germer, K., Lindenmaier, F., Färber, A., and Zehe, E.: Applied tracers for the observation of subsurface stormflow at the hillslope scale, HYDROLOGY AND EARTH SYSTEM SCIENCES, 13, 1145–1161, doi:10.5194/hess-13-1145-2009, 2009.

Wrede, S., Fenicia, F., Martínez-Carreras, N., Juilleret, J., Hissler, C., Krein, A., Savenije, H. H. G., Uhlenbrook, S., Kavetski, D., and Pfister, L.: Towards more systematic perceptual model development: a case study using 3 Luxembourgish catchments, HYDROLOGICAL PROCESSES, 29, 2731–2750, doi:10.1002/hyp.10393, 2015.

Zehe, E., Maurer, T., Ihringer, J., and Plate, E.: Modeling water flow and mass transport in a loess catchment, PHYSICS AND CHEMISTRY OF THE EARTH PART B-HYDROLOGY OCEANS AND ATMOSPHERE, 26, 487–507, doi:10.1016/S1464-1909(01)00041-7, 2001.

Zehe, E., Ehret, U., Blume, T., Kleidon, A., Scherer, U., and Westhoff, M.: A thermodynamic approach to link self-organization, preferential flow and rainfall-runoff behaviour, HYDROLOGY AND EARTH SYSTEM SCIENCES, 17, 4297–4322, doi:10.5194/hess-17-4297-2013, 2013.

Zehe, E., Ehret, U., Pfister, L., Blume, T., Schroder, B., Westhoff, M., Jackisch, C., Schymanski, S. J., Weiler, M., Schulz, K., Allroggen, N., Tronicke, J., van Schaik, L., Dietrich, P., Scherer, U., Eccard, J., Wulfmeyer, V., and Kleidon, A.: HESS Opinions: From response units to functional units: a thermodynamic reinterpretation of the HRU concept to link spatial organization and functioning of intermediate scale catchments, HYDROLOGY AND EARTH SYSTEM SCIENCES, 18, 4635–4655, doi:10.5194/hess-18-4635-2014, 2014.